Chinese Chemical Letters 33 (2022) 4213–4218

Contents lists available at ScienceDirect

Chinese Chemical Letters

journal homepage: www.elsevier.com/locate/cclet

Achieving blue water-dispersed room-temperature phosphorescence of carbonized polymer dots through nano-compositing with mesoporous silica

Chengyu Zheng, Songyuan Tao, Yang Liu, Chunyuan Kang, Bai Yang*

State Key Laboratory of Supramolecular Structure and Materials, College of Chemistry, Jilin University, Changchun 130012, China

ARTICLE INFO

Article history:
Received 28 November 2021
Revised 6 March 2022
Accepted 9 March 2022
Available online 13 March 2022

Keywords:
Carbonized polymer dots
Mesoporous silica
Nano-composite
Blue room-temperature phosphorescence
Water dispersion

ABSTRACT

Stabilizing triplet excited states is important for room temperature phosphorescence (RTP) materials to achieve multifunctional applications in humid environment. However, due to the lack of preparation strategies, the realization of RTP materials in water still faces challenges. Herein, a new design strategy was presented to achieve RTP in water by confining carbonized polymer dots (CPDs) in amino functional mesoporous silica (MSNs-NH_2). The as-prepared MSNs-CPDs aqueous dispersion exhibited blue afterglow, lasting more than 3 s to naked eyes. The triplet excited states were protected from non-radiative deactivation by the double-confinement effect including covalent bonding fixation and mesoporous structure confinement. The MSNs-CPDs inherited the structure of MSNs-NH_2, so the stability of morphology and properties were superior to CPDs and even most of silica-based CPDs RTP materials. A water-related encryption technique demonstrated the promising application of MSNs-CPDs as smart materials in the field of information security. Besides, the possibility of potential application in ion detection was also explored.

© 2022 Published by Elsevier B.V. on behalf of Chinese Chemical Society and Institute of Materia Medica, Chinese Academy of Medical Sciences.

Phosphorescence is a phenomenon of delayed luminescence, with long-lived triplet excited states. Room temperature phosphorescence (RTP) materials have attracted widespread attention, due to the unique advantage of large stokes shift, high signal-to-noise ratio, milliseconds or seconds lifetime and elimination of background emission interference. In recent years, RTP materials have been widely used in the field of anti-counterfeiting [1,2], information encryption [3,4], sensors [5,6], bioimaging [7] and optoelectronics [8–11], *etc.* Current RTP materials mainly contain rare earth inorganics [12,13], metal-organic complexes [14,15] or crystalline pure organic compounds [16,17]. However, these materials suffer from high toxicity, environment damage, high cost and complicated synthesis. It is urgent to develop new classes of metal-free RTP materials.

Carbonized polymer dots (CPDs) are emerging carbon-based luminescent nanomaterials [18–22], that are expected to solve the problems of traditional RTP materials. Generally, the CPDs-based RTP emission can be induced through the two following methods: one is the self-protective CPDs, the other is embedding CPDs into matrix [23–25]. The RTP of self-protective CPDs usually attribute to the highly crosslinked polymer structure, which is called crosslink-enhanced emission (CEE) [26,27]. Moreover, various matrices are introduced to construct matrix-assisted RTP CPDs, such as polyvinyl alcohol [28], polyurethane [29], boric acid [30], cyanuric acid [31] and inorganic salt [32]. Hydrogen bonds or covalent bonds among the matrices and CPDs can restrict the intermolecular motions and rigidify the triplet states of CPDs, thus inducing the RTP emission.

Notably most of CPDs-based RTP can only be observed in their dry solid state but quenched once exposed to water, that hinders the applications in humid environment. Therefore, it is necessary to achieve efficient RTP of CPDs-based materials in the existence of water. Very recently, some researchers covered CPDs with silica to protect the RTP in dispersion/aqueous solution. Liu's group presented a method for realizing RTP in water by incorporating carbon dots (CDs) into a three-dimensional silica network [33]. Then, Liu's group reported another method by anchoring CDs onto nanosilica [34]. Shan's group achieved RTP in aqueous solution by confining water-soluble CDs in a silica capsulation layer nanospace [35]. Although these reports realized CPDs-based RTP in aqueous media, there were still some nonnegligible problems: (1) Colloidal silica was widely applied to protect RTP of CPDs. While, the colloidal silica would further hydrolyze after freeze-drying or evaporation. The morphology would be changed in these processes and the powder could not be redispersed in water. So these materials were unsta-

* Corresponding author.
E-mail address: byangchem@jlu.edu.cn (B. Yang).

https://doi.org/10.1016/j.cclet.2022.03.041
1001-8417/© 2022 Published by Elsevier B.V. on behalf of Chinese Chemical Society and Institute of Materia Medica, Chinese Academy of Medical Sciences.

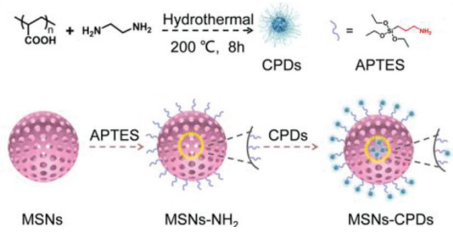

Scheme 1. Schematic illustration of the synthetic procedure of MSNs-CPDs.

ble in a sense. (2) The multifunctional CPDs was encapsulated inside the matrix through covalent bonds or supramolecular interactions and was isolated from external environment, which limited further functionalizations and applications. (3) There was still a lack of effective strategies to synthesis of CPDs-based RTP materials in aqueous solution. Therefore, it remained challenge to propose a new strategy to prepare CPDs-based RTP materials in aqueous environment.

Herein, we put forward a strategy based on double-confinement effect to synthesis water-dispersed CPDs-based RTP materials. We chose PAA-EDA CPDs [36] as the origin of RTP and amino functional mesoporous silica (MSNs-NH_2) as a matrix to protect the RTP in water. The as-prepared MSNs-CPDs (details were described in Experimental Section in Supporting information) aqueous dispersion showed blue afterglow, lasting more than 3 s to naked eyes. Different from the CPDs which was encapsulated in colloidal-silica, the as-prepared MSNs-CPDs displayed stable morphology and the powder obtained after freeze-drying could be redispersed in water. Due to being fixed to the surface and mesoporous channel of MSNs-NH_2, the CPDs could contact with the outside environment, which was beneficial for potential applications. Subsequently, we proposed double-confinement effect, consisting covalent bonding fixation and mesoporous structure confinement to explain how the MSNs-NH_2 protected the RTP of CPDs from quenching in water. Based on the unique properties, MSNs-CPDs aqueous dispersion was applied to water-related information encryption. The promising application of MSNs-CPDs aqueous dispersion in ion detection was also explored.

The preparation of CPDs and MSNs-CPDs was briefly illustrated in Scheme 1. CPDs was synthesized according to our previous work. The PAA-EDA CPDs was sensitive to water and easy to dissolve in water. Once exposed to water, the RTP of CPDs would be quenched. Amino functional mesoporous silica nanoparticle (MSNs-NH_2) was chosen as matrix to protect the RTP of CPDs. Owing to the multifunctional surface, good stability and well-defined pore structure, MSNs-NH_2 was expected to prevent CPDs from resolving in water, thus stabilizing the triplet states of CPDs. Firstly, mesoporous silica (MSNs) was prepared by using CTAB as template and TEOS as silica source. Then through the condensation reaction between the Si-OH of MSNs and APTES, the MSNs was functionalized with amino to prepare MSNs-NH_2. Finally, after hydrothermal treating of MSNs-NH_2 and CPDs, the MSNs-CPDs was synthesized. Interestingly, the MSNs-CPDs displayed good dispersibility (Fig. S1 in Supporting information) in water and the MSNs-CPDs aqueous dispersion showed blue afterglow, lasting more than 3 s to naked eyes (Fig. 1a), confirming that MSNs-NH_2 successfully protected the RTP in water. In contrast to the CPDs, the MSNs-CPDs showed good water dispersed RTP property. Moreover, after freeze-drying to powder, MSNs-CPDs could redisperse in water to form uniform aqueous dispersion (Fig. S1c in Supporting information). Table S1 showed the phosphorescence lifetime of the MSNs-CPDs aqueous dispersion with different ratios of MSNs-NH_2 to CPDs. The phosphorescence lifetime of the MSNs-CPDs aqueous dispersion increased and then gradually decreased as the ratio increasing from 1:1 to 4:1. The phosphorescence lifetime of the MSNs-CPDs aqueous dispersion reached a maximum when the ratio of MSNs-NH_2 to CPDs was 2:1.

The morphology of MSNs-NH_2 and MSNs-CPDs were characterized *via* scanning electron microscope (SEM), dynamic light scattering (DLS) and transmission electron microscopy (TEM). As shown in Fig. S2 (Supporting information) and Fig. 1b, SEM images of the MSNs-NH_2 and MSNs-CPDs displayed well-dispersed nanoparticles with a wide size range from 50 nm to 140 nm (average diameters of about 100 nm) and 60 nm to 140 nm (average diameters of about 100 nm), respectively. The SEM results indicated that after hydrothermal treatment, the diameter of MSNs-CPDs was similar to MSNs-NH_2 and the morphology remained the same as MSNs-NH_2. As shown in Fig. 1c, DLS characterization indicated that the average hydrodynamic diameters were in the range of 142–295 nm for MSNs-NH_2 and 122–342 nm for MSNs-CPDs, which were larger than diameters measured by SEM due to the existence of the hydration layer on the nanoparticles. TEM image of MSNs-NH_2 showed clear porous structure (Fig. 1d). After hydrothermal treatment, the porous structure disappeared (Fig. 1e), which indicated that CPDs was successfully grafted on MSNs-NH_2.

Zeta potentials of CPDs, MSNs-NH_2 and MSNs-CPDs were examined to be −10.8 mV, 25.5 mV and −4.9 mV, respectively (Fig. 2a), which further revealed CPDs had been successfully grafted on the surface of MSNs-NH_2. The X-ray photoelectron spectroscopy (XPS) spectra displayed four typical peaks, which were assigned to O 1s (532 eV), N 1s (399 eV), C 1s (285 eV) and Si 2p (104 eV), respectively (Fig. 2b). The high-resolution XPS results of O 1s could be deconvoluted into three peaks, which were attributed to Si-O bonds (532.9 eV), C–O bonds (532.4 eV) and C=O bonds (531.9 eV) (Fig. S3c in Supporting information). The Si–O bonds were assigned to MSNs-NH_2 and the C=O bonds were assigned to CPDs. To investigate how the CPDs connected with MSNS-NH_2, FT-IR spectra were measured. As shown in the FT-IR spectra (Fig. 2c), the absorption peaks at 1650 cm^{-1} and 1550 cm^{-1} were assigned to C=O stretching vibration and N–H vibration, respectively. Compared with CPDs, the intensity ratio of C=O bonds to N–H bonds decreased from 1.089 to 0.986 for MSNs-CPDs. The FT-IR results confirmed that the functional groups of CPDs had reacted with MSNs-NH_2, indicating CPDs was connected with MSNs-NH_2 through covalent bonds. Next, the porous structure of MSNs-NH_2 and MSNs-CPDs were investigated. As shown in Fig. 2d, the N_2 adsorption-desorption results of MSNs-NH_2 and MSNs-CPDs both displayed typical IV isotherms curve with a H1 hysteresis loop, indicating the presence of ordered mesoporous channels. In contrast with MSNs-NH_2, surface area and pore volume of MSNs-CPDs decreased from 666.4 m^2/g to 144.8 m^2/g and 0.8313 cm^3/g to 0.5673 cm^3/g, respectively (Table S2 in Supporting information). The pore size distribution of MSNs-NH_2 was concentrated at about 2.0 nm, and the size distribution of CPDs after hydrothermal treatment ranged from 0.8 nm to 2.2 nm (Fig. S4 in Supporting information). Thus, CPDs could partially accessed into the mesoporous of MSNs-NH_2. The powder small-angle XRD (PXRD) was employed to further investigate the mesoporous structure of MSNs-NH_2 and MSNs-CPDs (Fig. 2e). The PXRD pattern of MSNs-NH_2 displayed two characteristic diffraction peaks, which corresponded to the (100) and (110) panel. The PXRD further confirmed MSNs-NH_2 possessed the ordered pore channel. But, after hydrothermal treatment, the characteristic diffraction peaks at (100) and (110) disappeared in MSNs-CPDs. Meanwhile, the characteristic diffraction peaks for CPDs at 22° appeared in MSNs-CPDs (Fig. S5 in Supporting information). After modification with CPDs, the regularity degree of MSNs-NH_2 reduced, indicating that CPDs partly access into mesoporous channel. These characterizations confirmed that through covalent bonds, CPDs was partly immobilized on the surface of MSNs-NH_2 and partly constrained into the mesoporous

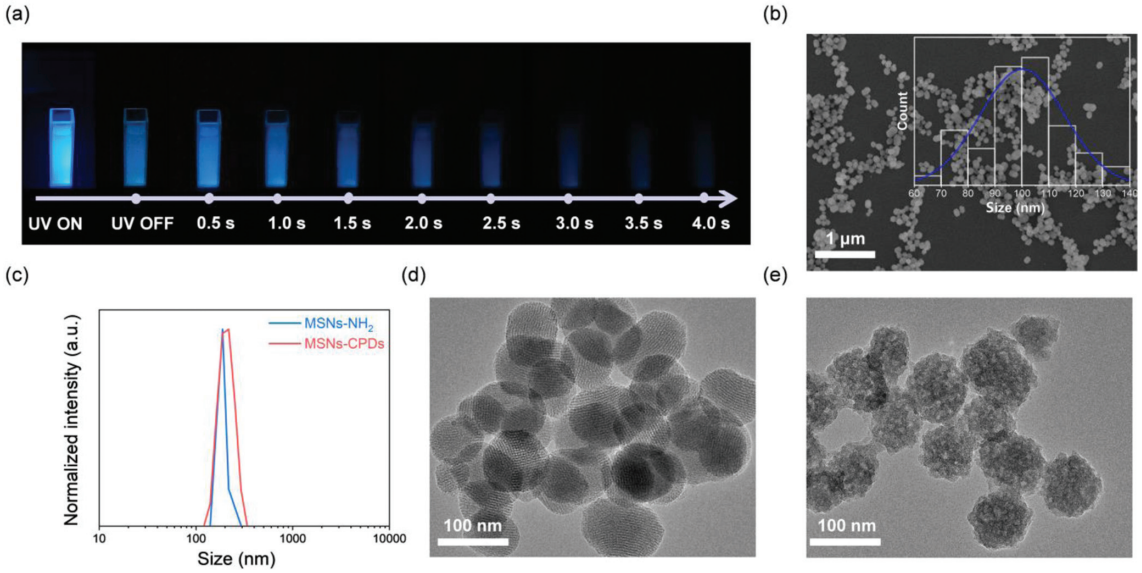

Fig. 1. (a) Photographs of MSNs-CPDs (10 mg/mL in water) at different delay time after UV irradiation. (b) SEM image of MSNs-CPDs (inset: particle size distribution). (c) Hydrodynamic diameter distributions of MSNs-NH_2 and MSNs-CPDs. (d) TEM image of MSNs-NH_2. (e) TEM image of MSN–CPDs.

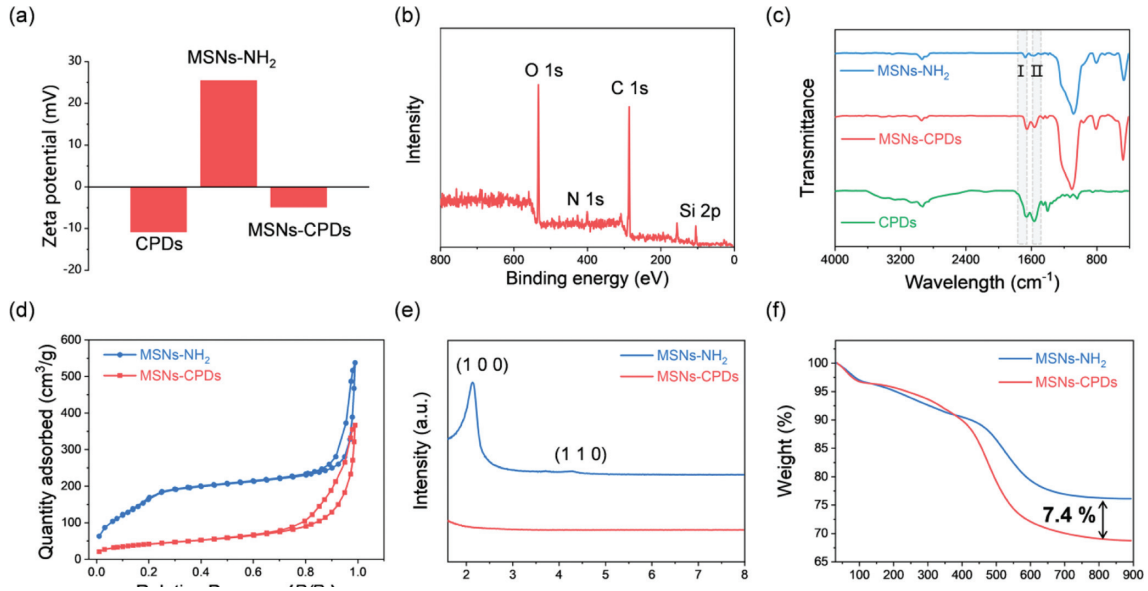

Fig. 2. (a) Zeta potentials of CPDs, MSNs-NH_2 and MSNs-CPDs. (b) XPS spectrum of MSNs-CPDs. (c) FT-IR spectra of MSNs-NH_2, MSNs-CPDs and CPDs. (d) N_2 adsorption-desorption isotherms. (e) Powder small-angle XRD patterns. (f) TGA curves of MSNs-NH_2 and MSNs-CPDs.

channel of MSNs-NH_2. Thermogravimetric analysis (TGA) results (Fig. 2f) demonstrated the total weight loss of MSNs-NH_2 and MSNs-CPDs were 24.0% and 31.4%, respectively. Thus, the doping weight of CPDs was calculated to be 7.4% for MSNs-CPDs.

The UV absorption spectrum of MSNs-CPDs displayed a wide peak ranging from 320 nm to 370 nm, which was attributed to the n-π^* transition of C=O/C=N bonds of CPDs (Fig. 3a). As shown in Fig. 3b, the photoluminescence (PL) spectra of MSNs-CPDs aqueous dispersion showed characteristic excitation-dependent fluorescence of CPDs. Under the excitation of 345 nm, the PL emission of MSNs-CPDs aqueous dispersion was strongest, centered at about 410 nm. Interestingly, MSNs-CPDs aqueous dispersion exhibited blue afterglow after turning off UV illumination (365 nm). The afterglow emission spectra of MSNs-CPDs revealed the phosphorescence emission behavior of MSNs-CPDs aqueous dispersion, centered at 430 nm (Fig. 3c). The quantum yield of MSNs-CPDs was 20.73% and the phosphorescence quantum yields were 6.00% in aqueous dispersion under excitation of 365 nm (Table S3 in Supporting information). The temperature-dependent RTP decay spectra of MSNs-CPDs aqueous dispersion (Fig. 3d) indicated that the afterglow delay lifetime decreased as temperature increased (Table S4 in Supporting information). Consequently, the spectra demonstrated that the afterglow was indeed RTP, rather than thermally activated delayed fluorescence. The RTP lifetime of MSNs-CPDs aqueous dispersion was determined from the RTP decay spectrum (Fig. 3e), which could be fitted by a double exponential function (Table S5 in Supporting information). Based on the following equation (Eq. 1), the average lifetime was calculated

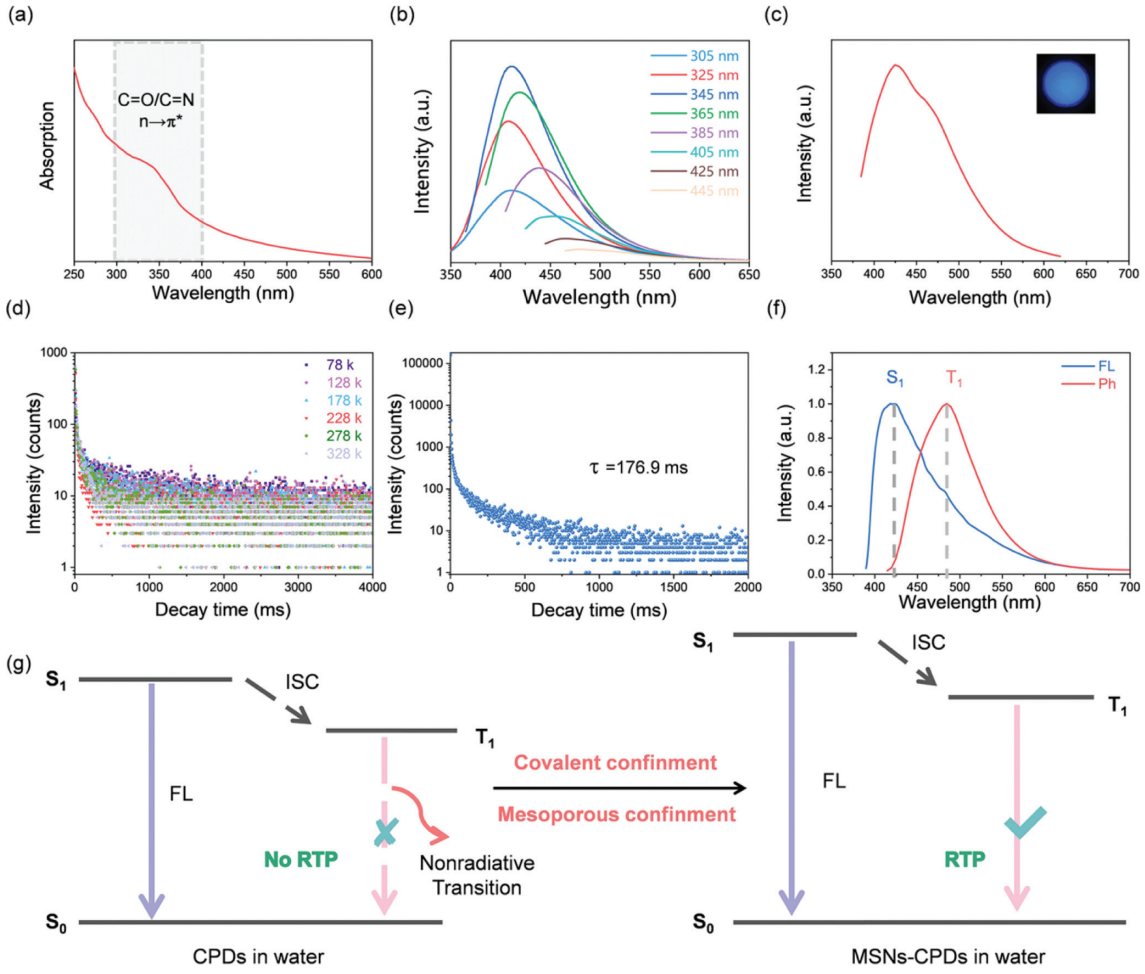

Fig. 3. (a) UV–vis absorption spectrum of MSNs-CPDs (10 mg/mL in water). (b) Excitation dependence PL spectra of MSNs-CPDs (10 mg/mL in water). (c) Phosphorescence emission spectrum of MSNs-CPDs (10 mg/mL in water) (inset: photograph of MSNs-CPDs aqueous dispersion after switching off UV). The emission spectrum was collected with the delay time of 3 ms. (d) Temperature-dependent RTP decay spectra of MSNs-CPDs (10 mg/mL in water). (e) RTP decay spectrum of MSNs-CPDs (10 mg/mL in water). (f) The steady-state photoluminescence spectrum (blue line) and phosphorescence emission spectrum (red line) of MSNs-CPDs excited under 365 nm at 77 K. The phosphorescence emission spectrum was collected with the delay time of 1 s. (g) Schematic illustration of the double-confinement effect mechanisms of the MSNs-CPDs in the aqueous solution.

to be 176.9 ms.

$$\tau_{ave} = \frac{\sum \partial_i \tau_i}{\sum \partial_i} \quad (1)$$

According to the steady-state photoluminescence spectra and phosphorescence emission spectra of MSNs-CPDs excited under 365 nm at 77 K, the energy gap (ΔE_{ST}) was calculated to be 0.34 eV (Fig. 3f).

The CPDs displayed phosphorescence quenching phenomenon in water. In contrast, after immobilizing CPDs in the MSNs-NH_2, MSNs-CPDs showed bright blue phosphorescence in aqueous solution (Fig. 1a), which demonstrated that MSNs-NH_2 could protect RTP of CPDs in water. What resulted in such a unique phenomenon was thoroughly explored and discussed. We performed contrast experiments to investigate the reason why the MSNs-NH_2 could prevent the RTP of CPDs from quenching in water. MSNs-$CPDs_I$ was synthesized by hydrothermal treatment of the mixture of MSNs and CPDs. MSNs-$CPDs_{II}$ was synthesized through mixing the MSNs-NH_2 (after hydrothermal treatment) and CPDs (after hydrothermal treatment) in room temperature. Both MSNs-$CPDs_I$ and MSNs-$CPDs_{II}$ aqueous dispersion displayed fluorescence (Fig. S6 in Supporting information) but almost no phosphorescence emission (Figs. S7, S8a and b, Table S6 in Supporting information). MSNs without active group (amino) was unable to react with CPDs to form new covalent bonds in MSNs-$CPDs_I$. Room temperature was insufficient to provide appropriate reaction condition for amino and carboxyl groups, so no new covalent bonds can be formed in MSNs-$CPDs_{II}$, either. These results confirmed that only the role of supramolecular interactions or physical adsorption was not able to protect phosphorescence, instead, covalent bonds played a decisive role in protecting phosphorescence in water. This was due to the fact that through covalent bonds the CPDs was effectively immobilized in MSNs-NH_2 and the vibration and rotation of CPDs were restricted in water. The covalent bonds stabilized the excited triplet states and prevented nonradiative decay, thus protecting the RTP in water [37]. Another contrast experiment was carried out to explore the role of mesoporous structure in protecting RTP. Amino-functional solid silica sphere without porous structure was prepared and then hydrothermal with CPDs to synthesis SiO_2-CPDs. SiO_2-CPDs showed both fluorescence and phosphorescence emission (Fig. S9 in Supporting information). Although the amino groups on the surface of SiO_2 could form covalent bonds with CPDs, the phosphorescence lifetime of SiO_2-CPDs was shorter compared with MSNs-CPDs (Figs. S8c and d, Table S6 in Supporting information). The results indicated that the mesoporous structure was equally important [38]. In according to these results, we put forward the double-confinement effect (Fig. 3g). The stable covalent bonds between MSNs-NH_2 and CPDs could efficiently immo-

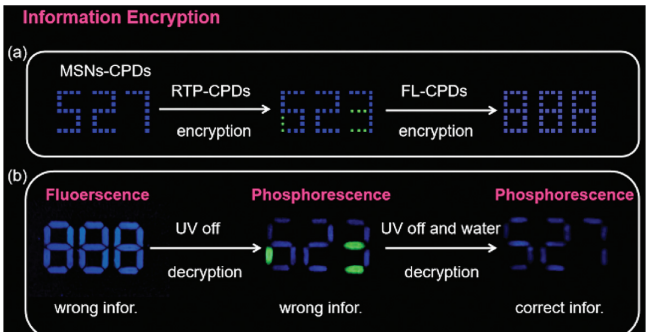

Fig. 4. (a) The schematic diagrams of information encryption. (b) Water-related multistage information encryption application of MSNs-CPDs.

bilize the CPDs. After immobilized in MSNs-NH_2, the intramolecular vibrations and rotations of CPDs were inhibited and the triplet states were stabilized in water by suppressing the nonradiative processes (Table S7 in Supporting information). The unique RTP property in aqueous solution of MSNs-CPDs was benefited from the covalent bonding fixation, which served as the first confinement effect. The size of the CPDs was a little smaller than mesoporous in MSNs-NH_2, so a proportion of CPDs was able to access the mesoporous structure. The mesoporous structure effectively confined the CPDs in nanoconfined space. The mesoporous structure confinement avoided the collision of water molecules, which prevented the nonradiative relaxation (Table S7) and stabilized the triplet states of CPDs, thus enabling the RTP in aqueous solution. The mesoporous confinement was the second confinement, which was also essential for protecting RTP in water. The double-confinement effect consisting of stable covalent bonding fixation and mesoporous structure confinement had a synergistic effect in suppressing the intramolecular vibration and rotation by suppressing the nonradiative processes (Table S7), thus successfully stabilizing the triplet excited states of the CPDs in water. RTP was effectively protected in water through the double-confinement effect.

The remarkable RTP of MSNs-CPDs inspired us to explore their potential applications in anti-counterfeiting and ion detection. Benefiting from the unique water dispersed RTP feature of MSNs-CPDs, we proposed a water-related information encryption and decryption strategy. The schematic diagram of information encryption was shown in Fig. 4a. We used the citric acid-EDA CPDs (FL ink) [39], PAA-EDA CPDs (RTP ink 1) and MSNs-CPDs aqueous dispersion (RTP ink 2) as inks, then handwrote the information with brush pen. Firstly, the right information “527” was written using the RTP ink 2. Subsequently, the “527” was performed to the first-stage encryption using the RTP ink 1 and turned into “623”. Finally, the “623” was performed to the second-stage encryption using the FL ink and became “888”. The information decryption was shown in Fig. 4b. The wrong information of “888” and “623” were observed either under 365 nm UV light or after the UV irradiation switching off. For decryption the information, the paper was first spray with water. Under the circumstances, the RTP of RTP ink 1 was quenched by water and the right information “527” was obtained by observing the RTP emission of RTP ink 2. The results confirmed that the MSNs-CPDs could be potentially applied in multi-level information protection systems. Since the CPDs was confined on surface and into mesoporous of MSNs-NH_2 and was able to contact with external environment, the MSNs-CPDs also could be used as a sensor for detecting metal ion in water media. Choosing Fe^{3+} as an example, we explored the possibility of MSNs-CPDs in ion detection. The results indicated that Fe^{3+} could induce a significant response to the phosphorescence and fluorescence of the MSNs-CPDs aqueous dispersion. The phosphorescence lifetime and the fluorescence intensity gradually decreased as the concentration of Fe^{3+} increasing. The linear relationships were obtained, with a correlation coefficient (R^2) of 0.97 for phosphorescence detection (Fig. S10 in Supporting information) and 0.8 for fluorescence detection (Fig. S11 in Supporting information). The detection limit for phosphorescence and fluorescence were respectively calculated to be 1.92 mmol/L and 1.56 mmol/L at a signal-to-noise ratio of 3. Compared with single fluorescence detection, dual detection based on fluorescence and phosphorescence appeared more accurate and persuasive [40]. The results distinctly demonstrated that MSNs-CPDs had a great potential for phosphorescence/fluorescence based detection in aqueous media.

In summary, the MSNs-CPDs was successfully developed by immobilizing CPDs on/into MSNs-NH_2. The as-prepared MSNs-CPDs with stable morphology displayed unique RTP in water and its dried powder could be redispersed in water. Further investigations revealed that the covalent bonds and mesoporous structure confined the CPDs to protect the triplet states of CPDs in water. Thus, we proposed the mechanism of the double-confinement effect, which was of great significance for the synthesis of CPDs-based RTP materials in water. We exhibited the application of MSNs-CPDs in water-related information encryption and explored the possibility of potential application in ion detection. MSNs-CPDs expanded the new perspective of the application of RTP materials in water. Detailed application of MSNs-CPDs in ion detection is still undergoing in our lab.

Declaration of competing interest

The authors declare that they have no known competing financial interests or personal relationships that could have appeared to influence the work reported in this paper.

Acknowledgment

This work was financially supported by the National Natural Science Foundation of China (NSFC, No. 22035001).

Supplementary materials

Supplementary material associated with this article can be found, in the online version, at doi:10.1016/j.cclet.2022.03.041.

References

[1] Y. Lei, W. Dai, J. Guan, Angew. Chem. Int. Ed. 59 (2020) 16054–16060.
[2] Q. Xiong, C. Xu, N. Jiao, Chin. Chem. Lett. 30 (2019) 1387–1389.
[3] Z. Yang, Z. Mao, X. Zhang, Angew. Chem. Int. Ed. 55 (2016) 2181–2185.
[4] H. Sun, S. Liu, W. Lin, Nat. Commun. 5 (2014) 3601.
[5] S.M. Borisov, R. Pommer, J. Svec, J. Mater. Chem. C 6 (2018) 8999–9009.
[6] W. Li, Y. Liu, B. Wang, Chin. Chem. Lett. 30 (2019) 2323–2327.
[7] H. Zhang, J. Jiang, P. Gao, ACS Appl. Mater. Interfaces 10 (2018) 17542–17550.
[8] P.K. Chow, G. Cheng, G.S.M. Tong, Chem. Sci. 7 (2016) 6083–6098.
[9] L. Xiao, Z. Chen, B. Qu, Adv. Mater. 23 (2011) 926–952.
[10] B. Wang, J. Li, Z. Tang, Sci. Bull. 64 (2019) 1285–1292.
[11] X. Yang, L. Sui, B. Wang, Sci. China Chem. 64 (2021) 1547–1553.
[12] V. Caratto, F. Locardi, G.A. Costa, ACS Appl. Mater. Interfaces 6 (2014) 17346–17351.
[13] T. Aitasalo, P. Dereń, J. Hölsä, J. Solid State Chem. 171 (2003) 114–122.
[14] Q. Zhao, F. Li, C. Huang, Chem. Soc. Rev. 39 (2010) 3007–3030.
[15] X. Yang, D. Yan, Adv. Opt. Mater. 4 (2016) 897–905.
[16] Z. An, C. Zheng, Y. Tao, Nat. Mater. 14 (2015) 685–690.
[17] W. Jia, Q. Wang, H. Shi, Chem. Eur. J. 26 (2020) 4437–4448.
[18] X. Xu, R. Ray, Y. Gu, J. Am. Chem. Soc. 126 (2004) 12736–12737.
[19] S. Tao, T. Feng, C. Zheng, J. Phys. Chem. Lett. 10 (2019) 5182–5188.
[20] C. Xia, S. Zhu, T. Feng, Adv. Sci 6 (2019) 1901316.
[21] S. Li, L. Li, H. Tu, Mater. Today 51 (2021) 188–207.
[22] B. Wang, J. Yu, L. Sui, Adv. Sci. 8 (2020) 2001453.
[23] P. Long, Y. Feng, C. Cao, Adv. Funct. Mater. 28 (2018) 1800791.
[24] K. Jiang, Y. Wang, X. Gao, Angew. Chem. Int. Ed. 57 (2018) 6216–6220.
[25] K. Jiang, Y. Wang, C. Cai, Adv. Mater. 30 (2018) e1800783.
[26] S. Zhu, Y. Song, J. Shao, Angew. Chem. Int. Ed. 54 (2015) 14626–14637.
[27] S. Tao, S. Zhu, T. Feng, Angew. Chem. Int. Ed. 59 (2020) 9826–9840.

[28] Y. Deng, D. Zhao, X. Chen, Chem. Commun. 49 (2013) 5751–5753.
[29] J. Tan, J. Zhang, W. Li, J. Mater. Chem. C 4 (2016) 10146–10153.
[30] W. Li, W. Zhou, Z. Zhou, Angew. Chem. Int. Ed. 58 (2019) 7278–7283.
[31] Q. Li, M. Zhou, M. Yang, Nat. Commun. 9 (2018) 734.
[32] C. Wang, Y. Chen, T. Hu, Nanoscale 11 (2019) 11967–11974.
[33] W. Li, S. Wu, X. Xu, Chem. Mater. 31 (2019) 9887–9894.
[34] J. He, Y. Chen, Y. He, Small 16 (2020) e2005228.
[35] Y. Liang, S. Gou, K. Liu, Nano Today 34 (2020) 100900.
[36] S. Tao, S. Lu, Y. Geng, Angew. Chem. Int. Ed. 57 (2018) 2393–2398.
[37] K. Jiang, Y. Wang, C. Cai, Chem. Mater. 29 (2017) 4866–4873.
[38] H. Zhang, B. Wang, X. Yu, Angew. Chem. Int. Ed. 59 (2020) 19390–19402.
[39] S. Zhu, Q. Meng, L. Wang, Angew. Chem. Int. Ed. 52 (2013) 3953–3957.
[40] J. Tan, Y. Ye, X. Ren, J. Mater. Chem. C 6 (2018) 7890–7895.